Long term interannual monitoring of open-ocean deep convection using altimetry and ocean color multi-sensors satellite data : case study of the Northwestern Mediterranean Sea.

Marine Herrmann[1], Pierre-Amael Auger[2], Caroline Ulses[3] and Claude Estournel[3]

[1]LEGOS, Université de Toulouse, IRD, CNES, CNRS, UPS, Toulouse, France

[2]Instituto Milenio de Oceanografa and Escuela de Ciencias del Mar, Ponticia Universidad Catlica de Valparaso, Valparaso, Chile

[3]Laboratoire d'Aérologie, Université de Toulouse, CNRS, UPS, Toulouse, France

Abstract. Deep convection occurs in a few regions of the world ocean submitted to strong atmospheric buoyancy loss and is at the origin of the formation of deep water masses (DWF) of the ocean circulation. It shows a strong interannual variability, and could drastically weaken under the influence of climate change. In this study, a method is proposed to monitor quantitatively deep convection using multi-sensors altimetry and ocean color satellite data, and applied and evaluated for the well observed DWF case study of Northwestern Mediterranean Sea (NWMS). that, a coupled hydrodynamical-biogeochemical numerical simulation is used to examine the signature of DWF on sea level anomaly (SLA) and surface chlorophyll concentration in the NWMS. Statistically significant correlations between DWF annual indicators and the areas of low surface chlorophyll concentration and low SLA in winter are obtained, and linear relationships between indicators and areas are established. They are applied to areas computed from altimetry 27-year and ocean color 19-year satellite datasets, producing the first long time series from observations of NWMS DWF indicators covering the last 2 decades. Model biases and smoothing effect induced by the low resolution of gridded altimetry data are partly taken into account by using corrective methods. Comparison with winter atmospheric heat flux and previous modeled and observed estimates of DWF indicators suggests that the DWF indicators time series obtained from standard ocean color products and altimetry capture realistically the interannual variability of the NWMS DWF. The interest but also weaknesses and uncertainties of the method are finally discussed.

1. Introduction

Open-ocean deep convection occurs in a few regions of the world ocean submitted to strong surface buoyancy losses that induce an increase of sea surface water density, resulting in the vertical mixing of the water column. It is at the origin of the formation of deep water masses of the ocean circulation [*Marshall and Schott*, 1999]. It shows a strong interannual variability [*Yashayaev*, 2007; *Herrmann et al.*, 2010], with mixing layer reaching depths varying within the full range from surface to sea bottom. Both observational and modeling studies suggested that it could drastically weaken under the influence of climate change [*Somot et al.*, 2006; *de Lavergne et al.*, 2014].

Northwestern Mediterranean Sea (NWMS) is one of the areas of dense water formation (DWF) : in this region, DWF occurs in winter under the influence of cold northerly winds and results in the formation of Western Mediterranean Deep Water, one of the main water masses of the Mediterranean thermohaline circulation. DWF in the NWMS does not only play an important role in the hydrodynamical functioning of the Mediterranean sea, it also influences the ecosystems: the associated winter vertical mixing is responsible for the nutrients enrichment of the surface layer, and therefore contributes to the following spring bloom [*Herrmann et al.*, 2013, 2014]. As a result, NWMS is one of the biologically most productive area of the Mediterranean sea [*Bosc et al.*, 2004]. Finally, due to its easier access compared to other convection regions (e.g. Labrador and Greenland seas), NWMS can be considered as a DWF golden case study.

Understanding and monitoring DWF interannual variability and long term evolution is essential for studies of ocean circulation and ecosystems, but long term in-situ monitoring of deep convection is costly. We therefore explore the possibility to monitor DWF using satellite data. First, as can be seen in altimetry data during the strong convection winter of 2005 (Fig. 1), DWF is associated to a lowering of sea surface due both to an increase of the water density (steric effect) and to an activation of the cyclonic circulation [dynamic effect, *Herrmann et al.*, 2008]. This influence of DWF on sea surface level was the starting point of studies that proposed methods to observe DWF using altimetry satellite data [*Herrmann et al.*, 2009; *Gelderloos et al.*, 2013]. For the NWMS, *Herrmann et al.* [2009] used alongtrack data from the altimetry track that crosses the deep convection area, using the results of a numerical oceanic simulation performed over the Mediterranean Sea to establish a relationship between sea level and DWF. Second, DWF is also associated to strong vertical displacements that induce the decrease of surface chlorophyll concentration [*Herrmann et al.*, 2013]. Since phytoplancton can not stay stably in the surface euphotic layer (where photosynthesis can occur), primary production stops (light limitation effect). Moreover, the initial chlorophyll stock present in the surface layer is vertically diluted throughout the whole mixed column [dilution effect, *Auger et al.*, 2014]. DWF consequently has a signature on surface chlorophyll concentration that can be observed on ocean color satellite data (see for example the strong convection winter of 2005, Fig. 1), suggesting that those data could be used to detect and monitor DWF.

Several authors attempted to use the chlorophyll depleted area estimated from satellite data as an indicator of deep convection intensity. These studies focused on individual cases or short time series of DWF. *Herrmann et al.* [2010] used it qualitatively to estimate the ability of their model to represent correctly the spatial extension convection for winter 2005. *Somot et al.* [2016] used this area as an indicator of DWF intensity for winters 2007 to 2013. Some authors multiplied empirically this area by the bottom depth (~2200 m) to provide estimates of the volume of dense water formed during respectively winter 2012 [*Durrieu de Madron et al.*, 2013] and winters 2007 to 2013 [*Houpert et al.*, 2016]. These latter studies therefore assumed that when and where convection occurs, it reaches the bottom. Their method is therefore only suitable for cases of either null or bottom convection, but not for intermediate convection cases.

Here, based on the results of a coupled hydrodynamical-biogeochemical ocean simulation, we propose a method to monitor annual DWF intensity on the long term using both altimetry and ocean color satellite observations for the case of NWMS. The numerical tool and satellite datasets as well as the existing estimations of DWF rates are presented in Sec. 2. We use the model to establish relationships between the DWF intensity on one side and the SLA and surface chlorophyll concentration on the other side, and obtain statistically significant relationships under the form of linear equations (Sec. 3). We then apply those equations to SLA and surface chlorophyll concentration obtained from real satellite data. This allows us to produce long-term time series of annual DWF intensity in terms of volumes of mixed water and newly formed dense water and mixed layer depth (Sec. 4). Advantages and weaknesses of our method and uncertainties that can affect those time series are discussed in Sec. 5, and concluding remarks are given in Sec. 6.

2. Tools : model, satellite datasets, existing estimations of DWF rates

2.1. The numerical model and simulations

A 38-year hydrodynamical simulation was performed over the western Mediterranean (0°40'W -11°40'E ; 36°25'N - 44°25'N, see Fig. 2) for the period 1975-2013 with the 3-D primitive equations, sigma-coordinate (40 levels), free surface ocean model SYMPHONIE

[*Marsaleix et al.*, 2009] at 2.5 km resolution. This resolution enables to reproduce realistically NWMS deep convection and associated mesoscale structures [*Herrmann et al.*, 2008]. The free surface scheme is the explicit non linear scheme detailed in *Marsaleix et al.* [2008]. The model was initialized and forced at the lateral boundaries by the results of a Mediterranean basin scale simulation performed with the NEMOMED8 model [*Herrmann et al.*, 2010] and at the surface by the atmospheric fluxes of the ARPERA dataset [*Herrmann and Somot*, 2008].

A twin tridimensional biogeochemical 38-year simulation was performed for the same period by forcing the biogeochemical model Eco3m-S using the results of the hydrodynamical simulation. This biogeochemical simulation is described in details in [*Auger et al.*, 2014] and the hydrodynamical and biogeochemical simulations were examined and validated by [*Auger et al.*, 2014; *Ulses et al.*, 2016]. This coupled hydrodynamical-biogeochemical tool was also used to study the impact of interannual variability and long-term evolution of atmospheric and oceanic conditions, in particular deep convection, on the NWMS pelagic planktonic ecosystem and associated carbon cycle [*Herrmann et al.*, 2013, 2014; *Ulses et al.*, 2016]. The studies cited here showed that our coupled model represents realistically NWMS ocean dynamics, in particular deep convection, as well as the interactions between this dynamics and the biogeochemistry.

Due to the Boussinesq approximation, SYMPHONIE is not able to reproduce the temporal variability of sea level associated to the steric effect. *Greatbatch* [1994] showed that sea level calculated by models making the Boussinesq approximation can be corrected for this problem by adding to the modeled sea level field a spatially uniform but time dependent constant that accounts for any net expansion/contraction of the global ocean.

To compute this temporally varying constant, we use the same method as *Lombard et al.* [2005] and *Bouffard et al.* [2008], using the monthly temperature and salinity fields from the NEMOMED8 simulation over the region between 2.5°E and 9°E, north of 39.5°E. We then remove the long term linear trend of the modeled sea level over the 1975-2013 period in order to remove the large scale sea level drift signal.

To quantify the intensity of DWF in the NWMS, we define several indicators. First, the maximum over the winter of the depth reached by the mixed layer (MLD) is an indicator of the DWF intensity widely used in modeling and observations studies. We consequently define the annual mean MLD over the convection area, MLD_{mean}, as :

$$MLD_{mean} = max_{t \in DJFM} \left(\frac{\iint_{(x,y) \in NWMS/MLD(x,y,t)>500} MLD(x,y,t)\, dx\, dy}{\iint_{(x,y) \in NWMS/MLD(x,y,t)>500} dx\, dy} \right) \quad (1)$$

where DJFM stands for the December-March winter period and NWMS is defined as the region between 2.5°E and 9°E and north of 39.5°N (see Fig. 2). We consider values of MLD larger than 500 m to ensure that we are in the convection area. In the model, the MLD is defined using a threshold value of 4 $cm^2.s^{-1}$ for the vertical diffusion coefficient [*Herrmann et al.*, 2008].

Second, the volume of water affected each year by DWF is also an indicator of its intensity, and is a key value for studying the formation and fate of water masses involved in the thermohaline circulation. Following previous studies (see Section 2.3), we consider two kinds of yearly volumic DWF indicators, as defined in *Herrmann et al.* [2008] : the maximum volume of mixed water, V_{MLD}, and the rate of dense water formed annually, $\tau_{29.11}$. V_{MLD} is the winter maximum of the spatial integral of the MLD over the convection area :

$$V_{MLD} = max_{t \in DJFM} \left(\iint_{(x,y) \in NWMS/MLD(x,y,t)>500} MLD(x,y,t)\, dx\, dy \right) \tag{2}$$

In our 38-year simulation, the densest water masses formed in winter have densities reaching 29.11 kg.m^{-3}, in agreement with values observed for 2012-13 (see Section 2.3) and with values from previous modeling studies and observations [reported for example in *Herrmann et al.*, 2010]. This value is therefore taken as the criterion to define the volume of dense water formed $V_{29.11}$, taken as the volume of water of density higher than $29.11 kg.m^{-3}$:

$$V_{29.11}(t) = \iiint_{(x,y,z) \in NWMS/\rho(x,y,z,t) \geq 29.11} dx\, dy\, dz \tag{3}$$

$\tau_{29.11}$ is then defined as the annual rate of dense water formed, computed as the difference between the maximum and the minimum during the winter of $V_{29.11}$:

$$\tau_{29.11} = max_{t \in DJFM}(V_{29.11}) - min_{t \in DJFM}(V_{29.11}) \tag{4}$$

Both volumic DWF indicators V_{MLD} and $\tau_{29.11}$ are quantified in Sv by dividing the cubic meters volumes by the number of seconds in one year. In the following, we therefore focus on three DWF indicators over the NWMS : MLD_{mean} (m), V_{MLD} (Sv), and $\tau_{29.11}$ (Sv). The time series of these three annual indicators computed from the model results are presented on Fig. 3 (gray curves).

2.2. Satellite data

2.2.1. Altimetry data

We use the L4 gridded SLA (Sea Level Anomaly) daily multi-missions satellite data generated at 1/4° resolution by the SSALTO/DUACS Delayed Time (DT) processing system for the period 1993 - 2015, and Near Real Time (NRT) processing system for

2016: a mapping procedure using optimal interpolation with realistic correlation functions is applied to produce SLA at a given date. These altimeter products cover the period 1993-2016 and are now distributed by the Copernicus Marine and Environment Monitoring Service (CMEMS, http://marine.copernicu.eu). The multi-satellite component of SSALTO/DUACS system is responsible for the production of processed HY-2A, Saral/AltiKa, Cryosat-2, Jason-1, Jason-2, Topex/Poseidon, Envisat, GFO, ERS1/2 and Geosat data in order to provide a homogeneous, inter-calibrated and highly accurate long time series of SLA altimeter data. As done for the modeled sea level, we remove from those data their linear long term trend. We also remove from both modeled and observed SLA their temporal averages over the period 1993-2016 in order to use the same reference for modeled and satellite sea level data.

2.2.2. Ocean color data

We use the standard L3 near-surface chlorophyll-a concentrations data computed daily from SeaWIFS (1998-2010) and MODIS (2003-2016) using the OC algorithm [*O'Reilly and et al.*, 2000] for the global ocean at a 9 km resolution (http://oceandata.sci.gsfc.nasa.gov).

2.3. In-situ data and existing estimations of deep water formation rate

Between summer 2012 and summer 2013, four oceanographic cruises were conducted in the NWMS in the framework of the MERMEX (Marine Ecosystems Response to climatic and anthropogenic forcings in the Mediterranean), HYMEX (Hydrological Cycle of the Mediterranean Experiment), DEWEX (Impacts of Deep water formation on the Mediterranean pelagic ecosystems) and MOOSE (Mediterranean Ocean Observing System Experiment) programs : July-August 2012 and February, April and June 2013. They are presented in details in *Testor* [2013] and *Conan* [2013].

A large set of CTD profiles (in average 70 per cruise) were collected during each of these cruises. One of the main goals of those cruises was to estimate the seasonal and annual variations of dense water volume. Based on the hydrographic in-situ CTD profiles that were collected, several estimations of the DWF rate were computed for winter 2012-13. Performing optimal interpolation of those profiles and using a numerical model to assess the uncertainty of the associated DWF rate estimates, *Waldman et al.* [2016] obtained a DWF rate of 2.3 $\pm$0.5 Sv for $\tau_{29.11}$. Performing objective analysis of those profiles combined with other in-situ data available over this period from gliders, ARGO floats, and moorings, *Bosse* [2015] proposed a 2 Sv DFW rate for $\tau_{29.11}$.

Several studies attempted to estimate the DWF rate for winter 2012-13 using other sources, i.e. numerical model results or satellite data. *Estournel et al.* [2016] used the SYMPHONIE model at 1 km resolution to perform a realistic numerical simulation that closely reproduces the observed characteristics of the water column during 2012-13, obtaining a 1.6 Sv rate for $\tau_{29.1125}$. Using the oceanic model NEMO at 1/36° resolution, *Léger et al.* [2016] ran three sensitivity experiments varying the initial ocean state and obtained DWF rates varying between 0.6 Sv and 2.6 Sv for $\tau_{29.11}$. *Houpert et al.* [2016] used 8-day L3 MODIS Aqua surface chlorophyll concentration satellite data to estimate DWF rates for the period 2007-2013 : they take the maximum extension of the low concentration area (defined with a threshold criteria of 0.15 mgChl.m^{-3}) and assume that the mean MLD below this area was 2200 m. This results in the following values for the years between respectively 2007 and 2013 : 0 Sv, 0 Sv, 1.14 Sv, 0.91 Sv, 1.10 Sv, 1.25 Sv, 1.65 Sv.

Previous observations and modeling studies also identified stronger than the average DWF winters : 1999 [*Béthoux et al.*, 2002, from in-situ observations], 2005 [*Herrmann et al.*, 2010, gave an estimate of 1.2 Sv from model results and suggested that winter 2005 was the most convective over the period 1960-2006 due to considerable atmospheric heat loss], 2006 [*Schroeder et al.*, 2008, gave an estimate of 2.4 Sv for winters 2005 + 2006 from in-situ observations], 2012 [*Durrieu de Madron et al.*, 2013, gave an estimate of 1.1 Sv from satellite color data using the same method as *Houpert et al.* [2016] with a threshold criteria of 0.1 mgChl.m^{-3}]. *Somot et al.* [2016] performed a simulation over the Mediterranean Sea for the 1980-2013 period using a coupled ocean-atmosphere model (ALADIN-Climate - NEMOMED8) to investigate the factors responsible for the interannual variability of deep convection. In their paper, they produced a time series of DWF rate (their Fig. 6), identifying winter 2005 as the most convective of the period.

3. Signature of deep convection on sea surface color and height in the coupled simulation.

To assess the DWF annual intensity using satellite color and altimetry data, we first need to establish relationships between the sea surface characteristics and the intensity of deep convection. In this section, we use the 38-year coupled hydrodynamical-biogeochemical simulation to establish relationships between the surface chlorophyll concentration on one side and the DWF indicators on the other side, and the 38-year hydrodynamical simulation to establish relationships between the SLA on one side and the DWF indicators on the other side.

3.1. From sea surface color to dense water formation

As explained above, very low chlorophyll concentration values are observed during the period and over the surface of DWF (see the example of winter 2005 on Fig. 1 and 6, the most convective year over the simulated period as can be seen on Fig. 3). We therefore look for relationships between the size of the chlorophyll depleted area, A_{lowCHL}, and the indicators of DWF intensity defined above. For a given period T and a given surface chlorophyll concentration threshold Chl_{crit}, A_{lowCHL} is defined as the surface area where the chlorophyll concentration averaged over the period T is lower than Chl_{crit} :

$$A_{lowCHL} = \iint\limits_{(x,y)\in RDC/(\int\limits_{t\in T} Chl(x,y,t)dt)\leq Chl_{crit})} dx\, dy. \tag{5}$$

where (x, y) belongs to the region RDC (Region of Deep Convection) of the NWMS where DWF occurs in the model and low chlorophyll concentrations are observed in the model and satellite data : we consider the region between 2.5°E and 9°E, north 40°N and of a line going from [40°N;4.5°E] to [42°N;9°E]. Since we study open ocean convection and not shelf dense water formation, we also put a constraint on the depth, considering only the region where it exceeds 1000 m. The selected region (see black line on Fig. 1, 2 and 6) is consistent with the "blooming" bio-region defined by *D'Ortenzio and Ribera d'Alcalà* [2009] who applied a K-means cluster analysis on time series of chlorophyll concentration computed from SeaWIFS satellite data to characterize the biogeography of the Mediterranean Sea.

To compute annual time series of A_{lowCHL}, we then need to define the period of averaging T and the chlorophyll surface concentration criteria Chl_{crit}. For that, we use a simple optimization procedure, varying T inside the January-March period (during which DWF occurs), and varying the value of Chl_{crit} in the range [0.00-1.00] mgChl.m^{-3}. We finally select the period and chlorophyll concentration criteria for which we obtain the highest correlations between the annual time series of DWF intensity indicators and A_{lowCHL}. For V_{MLD} and $\tau_{29.11}$, this is obtained for the period of days 25-80, i.e. January 25th - March 20th or 21st, and for Chl_{crit} = 0.35 mgChl.m^{-3}, and we obtain statistically significant correlations (significant level SL >0.9999) of respectively 0.88 and 0.89 with A_{lowCHL} (Fig. 7). For MLD_{mean}, this is obtained for the period of days 25-72, i.e. January 25th - March 12th or 13th, for Chl_{crit} = 0.50 mgChl.m^{-3}, with a statistically significant correlation (SL >0.9999) of 0.64 with A_{lowCHL} (Fig. 7). Given these high correlation levels, we then perform linear regression analysis under the form $y = ax + b$ where y is the value of the DWF indicator and x is the value of A_{lowCHL} : the values of a and b are given for each DWF indicator on Fig. 7. When quantifying the DWF indicators in m^3 instead of Sv, the values of a are respectively equal to 751 m and 1057 m for V_{MLD} and $\tau_{29.11}$, much smaller than the 2200 m value used by *Durrieu de Madron et al.* [2013] and *Houpert et al.* [2016]. We finally apply those linear relationships to the values of A_{lowCHL} given by the model to obtain time series of V_{MLD}, $\tau_{29.11}$ and MLD_{mean} predicted from those relationships. Those time series are presented on Fig. 3 (black curves). The normalized root-mean-square error (NRMSE) between the DWF indicators computed directly from the hydrodynamical simulation and those predicted values are respectively of 10.4%, 11.0% and 14.9% for V_{MLD}, $\tau_{29.11}$ and MLD_{mean}.

The 0.35 mgChl.m^{-3} value of Chl_{crit} obtained for the volumic DWF indicators can be qualitatively justified by considering the sea surface characteristics for winter 2005 in the model (Fig. 6) : the area of deep convection (where MLD >500 m) is approximately the same as the area inside the 0.35 mgChl.m^{-3} isoline for the surface chlorophyll concentration averaged over January 25th - March 21st.

The strong correlation obtained in the model between the volume of water affected by convection and the chlorophyll depleted area can be mainly explained by the vertical dilution effect of convection. Before winter convection, in October-November, the water column is still stratified, chlorophyll is mainly present in the surface euphotic layer, the total chlorophyll content of the water column is minimum, as well as its interannual variability (Fig. 8, left). When convection occurs, this initial chlorophyll content is diluted over the mixed column, the surface chlorophyll concentration should therefore be approximately inversely proportional to the convection depth. This inversely proportional pattern can be observed in the model on the scatterplot of daily values of MLD vs. surface chlorophyll concentration at the center of the convection area during the January-February period (Fig. 8, right), suggesting that the dilution effect is indeed the main factor responsible for the chlorophyll depletion of the surface water. Moreover, most of MLD values greater than $\sim$500 m are associated to chlorophyll surface concentration values lower than $\sim$0.35 mgChl.m^{-3} (Fig. 8, right). $\sim$0.35 mgChl.m^{-3} therefore approximately corresponds to the value below which the surface chlorophyll concentration falls when the mixed layer reaches significant depths, i.e. MLD $>\sim$500 m. The dilution effect therefore enables to physically justify the strong correlation found above, but also the 0.35 mgChl.m^{-3} threshold.

3.2. From sea surface height to dense water formation

Herrmann et al. [2009] used a 9-year simulation at $1/16° \sim 5$ km resolution and considered sea level data obtained along track 146 of altimetry data. Our goal is to strengthen the robustness of this relationship using a longer (38-year) simulation with a higher resolution (2.5 km), hence who represents more realistically deep convection spatial patterns. Moreover we use gridded altimetry data, where submesoscale structures, which are highly active during convection [*Herrmann et al.*, 2008], should be filtered out compared to along-track data. To establish relationships between the SLA and the DWF intensity indicators V_{MLD}, $\tau_{29.11}$ and MLD_{mean}, we proceed the same way as for the surface chlorophyll : we look for relationships between those indicators and the size of the low SLA area, A_{lowSLA}. For a given period T and a given surface chlorophyll concentration threshold Chl_{crit}, A_{lowSLA} is defined as the surface area where the SLA averaged over the period T is lower than SLA_{crit} :

$$A_{lowSLA} = \iint\limits_{(x,y)\in RDC/(\int\limits_{t\in T} SLA(x,y,t)dt)\leq SLA_{crit})} dx\,dy. \tag{6}$$

We consider the same RDC region as for the surface chlorophyll (black line on Fig. 6). We then vary the period T and the criteria SLA_{crit}, and choose those that maximise the correlations between the DWF indicators and A_{lowSLA}. The optimal averaging period is February 15th - March 15th, with SLA_{crit} of respectively -14.0 cm, -14.0 cm and -5.5 cm for V_{MLD}, $\tau_{29.11}$ and MLD_{mean}. We obtain statistically significant correlations (SL >0.9999) between these indicators and A_{lowSLA} of respectively 0.83, 0.77 and 0.75 (Fig. 7). Values of a and b obtained for each DWF indicator when performing linear regression analysis under the form $y = ax + b$ where y is the value of the DWF indicator and x is the value of A_{lowSLA} are given on Fig. 7. The NRMSE between the DWF indicators computed directly from the hydrodynamical simulation and their value predicted when applying these relationships to the modeled A_{lowSLA} are respectively of 13.5%, 15.1% and 12.8% for V_{MLD}, $\tau_{29.11}$ and MLD_{mean} (Fig. 7).

3.3. Using together sea surface height and chlorophyll concentration

To combine the information provided both by altimetry and ocean color data we also establish bi-linear relationships under the form $y = a_1x_1 + a_2x_2 + b$ where y is the value of the DWF indicator, x_1 is the value of A_{lowCHL} and x_2 is the value of A_{lowSLA}. The values of a_1, a_2 and b are indicated in blue on Fig. 7, as well as the correlation coefficients and NRMSE between the time series of DWF indicators given directly by the model and predicted using the bi-linear relationships. Those correlation coefficients are respectively equal to 0.879, 0.890, 0.754 (SL>0.999) and the NRMSE to 10.3%, 11.0% and 12.7%, for respectively V_{MLD}, $\tau_{29.11}$ and MLD_{mean}, only marginally higher than the best coefficients obtained for each indicator : 0.877 (NRMSE 10.4%), 0.886 (NRMSE 11.0%) and 0.748 (NRMSE 12.8%) obtained respectively with A_{lowCHL}, A_{lowCHL} and A_{lowSLA}. This is due to the fact that performing this multivariate regression analysis is we actually equivalent to applying a weighted average to both linear relationships $y = ax+b$ previously obtained. The strongest weight is given to the relationship associated to the highest predicted vs. direct modeled time series correlation, as can be seen when comparing the $y = a_1x_1 + a_2x_2 + b$ equation with both $y = ax + b$ equations on Fig. 7. In the model, for a given DWF indicator, multivariate DWF indicator time series, showed in black on Fig. 4, is therefore close from the univariate time series associated to the strongest weight (Fig. 3).

4. From satellite data to DWF intensity

To obtain DWF indicators time series from real satellite observations data, we apply to the areas of low SLA and low surface chlorophyll concentration computed from those data the $y = ax + b$ and $y = a_1x_1 + a_2x_2 + b$ relationships established for the model in Sec. 3. First we compare the modelled and satellite observed values in terms of SLA and surface chlorophyll concentration to determine how these relationships can be applied to real datasets, adjusting the criteria used to compute the areas of low surface chlorophyll concentration and SLA.

4.1. Adjustment of Chl_{crit} for ocean color data

Time series of the mean surface chlorophyll concentration and chlorophyll depleted area computed from the model and from altimetry over the RDC region are presented on Fig. 5. The length of the common period between ocean color data and the model is 12 years for SeaWIFS (no data in 2008) and 11 years for MODIS. The correlation factors between time series of the mean surface concentration over RDC and over the period January 25th - March 21st computed in the model and in the data are respectively of 0.59 (SL=0.96) and 0.76 (SL=0.99) for the period January 25th - March 21st, and 0.75 (SL=0.99) and 0.83 (SL>0.999) for the period January 25th - March 13th. The model overestimates this mean surface chlorophyll concentration compared to data : +0.17-0.18 mgChl.m^{-3} for SeaWIFS for the 1998-2010 period; +0.06-0.07 mgChl.m^{-3} for MODIS for the 2003-2013 period (Fig. 5).

Both satellite datasets show the same variability, being extremely similar in terms of correlation and values. We therefore merge those data to produce a long 19-year time series over the period 1998-2016 over which we will apply the relationships established from the model in Section 3. We have to account for the model overestimation. For that we adjust the chlorophyll concentration criteria Chl_{crit} used to compute A_{lowCHL}. For the model, Chl_{crit} =0.35 mgChl.m^{-3} as established in Section 3.1, both for the periods January 25th - March 21st and January 25th - March 13th. For the merged satellite dataset we vary Chl_{crit} and use the value that maximizes the temporal correlation and minimizes the NRMSE between A_{lowCHL} computed from the merged dataset and A_{lowCHL} computed from the model. This results in criteria Chl_{crit} of resp. 0.35 mgChl.m^{-3} and 0.50 mgChl.m^{-3} for resp. the periods January 25th - March 21st and January 25th - March 13th. Resulting correlations between the model and the merged dataset for A_{lowCHL} time series are respectively of 0.85 and 0.79 and highly significant (SL>0.999) for the respective periods January 25th - March 21st and January 25th - March 13th, with RMSE∼20% for both periods (Fig. 5).

4.2. Adjustment for altimetry data

Time series of the mean SLA over RDC from model and altimetry are presented on Fig. 9. Over the 1993-2013 period, the correlation between the altimetry data and the model of the SLA averaged over RDC and over the period February 15th - March 15th SLA_{mean} is equal to 0.41 (SL>0.94) with a mean bias of -0.4 cm and a NRMSE of 28.0% (Fig. 9). The model reproduces correctly the range of observed sea level values, but its representation of their interannual chronlology is not very good. There are two main reasons for that : the model does only represent the monthly variations of the steric effect (see Section 2.1) and therefore can miss its high frequency variations, contained in the altimetry data; the spatial and temporal resolution of the SLA tracks used to produce the SLA gridded dataset is not very high (∼10 days, O(100 km)), much smaller than in the model, also preventing altimetry to capture correctly the high frequency of the SLA spatial and temporal variability. As a result, SLA patterns are strongly smoothed in altimetry data, with spatial extrema less peaked than in reality and in the model, as can be seen on Fig. 1 and 6: regions of extrema are of larger extension but with weaker extrema values. This smoothing effect will therefore result in an overestimation of A_{lowSLA}. We need to account for this spatial smoothing effect when applying the linear relationship established in the model to the data. To do that, we apply a corrective factor C on A_{lowSLA}, computed by taking the ratio between the model A_{lowSLA} and the observed A_{lowSLA}, both averaged over 1993-2013 :

$$A_{lowSLA}^{altimetry,corrected}(y) = C \times A_{lowSLA}^{altimetry}(y)$$
$$\text{with} \qquad (7)$$
$$C = \frac{\overline{A_{lowSLA}^{model}}}{\overline{A_{lowSLA}^{altimetry}}}$$

where A_{lowSLA}^{model} and $A_{lowSLA}^{altimetry}$ are the values of the area computed respectively from the model and the altimetry taking the corresponding values of SLA_{crit}, $A_{lowSLA}^{altimetry,corrected}$ is the value obtained from the altimetry after applying the corrective factors, and the overbar denotes the average over the 1993-2013 period. For values of SLA_{crit} of respectively -14.0 cm and -5.5 cm, we obtain corrective factors C of respectively 5.629 and 0.888. The resulting time series of $A_{lowSLA} \times C$ is shown on Fig. 9 (red curve).

4.3. Time series of DWF indicators from real ocean color and altimetry datasets

After having computed time series of A_{lowCHL} and A_{lowSLA} from real datasets, we finally apply the $y = ax + b$ relationships established in the model to those real datasets time series. Time series obtained for V_{MLD}, $\tau_{29.11}$ and MLD_{mean} are shown on Fig. 3 and given in Tab. 1.

Previous observations and modeling studies (Sec. 2.3) provide a list of known strong DWF winters : 1999, 2005, 2006, 2012 and 2013. Winters of DWF stronger than the average given by ocean color data are 2004, 2005, 2006, 2010, 2013, 2015, and given by altimetry are 2003, 2005, 2012 and to a lesser extent 2009, 2011, 2014, 2015. Both types of data miss several strong DWF winters (2012 for color data, 2006, 2010 and 2013 for altimetry). This is discussed in the following (Sec. 5). Ocean color dataset gives 2005 as the most convective winter, as suggested in the literature [*Schroeder et al.*, 2008; *Herrmann et al.*, 2010; *Somot et al.*, 2016]. Altimetry ranks it as the second most convective winter, ranking 2012 as the most convective winter. To our knowledge, winter 2012-13 was the only winter for which the in-situ measurements coverage allowed to produce a robust rate of DWF (resp. 1.8 and 2.3±0.5 Sv for $\tau_{29.11}$ in *Bosse* [2015] and *Waldman et al.* [2016]). Our color data time series falls in this range, whereas altimetry data misses this convective winter (Fig. 3).

Herrmann et al. [2010] showed that the intensity of DWF was significantly correlated to atmospheric conditions during the DWF period, in particular to the average winter (December-February) heat loss over the NWMS, HL_{DJF}. Examining jointly HL_{DJF} time series with the DWF indicators time series obtained here therefore provides an indication about the DWF interannual variability and about the ability of the satellite data to reproduce correctly this variability. We compute HL_{DJF} for the period 1976-2016 using NCEP reanalysis outputs [*Kalnay et al.*, 1996, Fig. 3]. We then compute the correlation between the HL_{DJF} time series and the DWF indicators time series obtained from various methods (direct model, model SLA, satellite altimetry, model chlorophyll concentration and satellite ocean color, combined altimetry and ocean color, Tab. 2). The correlation between DWF indicators given directly by the 38-year simulation and HL_{DJF} is equal to respectively 0.68, 0.75 and 0.71 (SL>0.999) for V_{MLD}, $\tau_{29.11}$ and MLD_{mean} over the 1976-2013 period, confirming that the model reproduces realistically the interannual variability of DWF in the NWMS. The correlation between DWF volumic indicators V_{MLD} and $\tau_{29.11}$ predicted from the altimetry data with correction and HL_{DJF} is statistically significant, equal to 0.60 (SL>0.99) over the 1993-2016 24-year period. However the correlation is weaker and less significant for MLD_{mean} (0.45, SL=0.94). This will be discussed below (Section 5). The time series produced from ocean color merged dataset also shows a statistically significant correlation with HL_{DJF} (0.67 (SL>0.999), 0.69 (SL>0.999), 0.67 (SL<0.999) for V_{MLD},$\tau_{29.11}$ and MLD_{mean} over the 1998-2016 19-year period). This suggests that the method built there, using gridded altimetry data and standard ocean color data, allows to produce time series that correctly capture the interannual variability of DWF in the NWMS.

Somot et al. [2016] confirmed that winter buoyancy loss plays a key role, but also that the initial stratification of the water column influenced the convection, explaining that years with strong buoyancy loss show convection weaker than expected. For example in their simulation $\tau_{29.11}$ was 1/2 smaller for 2012 than for 2013 although the winter buoyancy loss was stronger. Though it provides an indication about the ability of satellite data to reproduce realistically DWF indicators time series, it should be underlined that the correlation between our DWF time series and NCEP HL_{DJF} must only be considered as an indication of the realism of those time series in terms of interannual variability, and not as an exact metric of this realism.

The time series obtained by applying the bi-linear relationships established in Sec. 3.3 are shown on Fig. 4 and given in Tab. 1, and the correlation coefficients between those time series and HL_{DJF} are given in Tab. 2. As explained in Sec. 3.3, those bi-linear relationships give the strongest weight to the area A_{lowCHL} or A_{lowSLA} for which the correlation between predicted and direct modeled DWF indicators time series is the strongest. As a result, for each indicator, the time series computed from combined altimetry and ocean color data is very similar to the time series obtained from the dataset associated to this strongest weight (ocean color for V_{MLD} and $\tau_{29.11}$, altimetry for MLD_{mean}) and the correlation with HL_{DJF} is weakly improved. For MLD_{mean}, the difference of coefficient for combined dataset (0.434) vs. altimetry (0.241) is only due to the fact that the period considered differs. For V_{MLD}, the correlation improvement is mainly due to the fact that altimetry overestimates DWF for 2012, correcting the fact that ocean color misses it.

5. Discussion

The advantage of the method developed here compared to empirically deduced relationships is the fact that it is based on the physical links reproduced by the numerical model between DWF, SLA and chlorophyll concentration. *Durrieu de Madron et al.* [2013] and [*Houpert et al.*, 2016] used chlorophyll satellite data to propose DWF rate estimates (see Sec. 2.3), however their method overestimates intermediate convection cases as explained in Sec. 1. Indeed, for years 2009-2013, the range of DWF rate proposed by *Somot et al.* [2016] (0.2 to 1.7 Sv for $\tau_{29.11}$) was larger, with same maximum value but lower weak and intermediate values, than the one proposed by *Houpert et al.* [2016] (0.9 to 1.7 Sv). Moreover, with this method, the day of maximum extension can be missed since the temporal coverage of the daily data is not perfect (we computed a temporal coverage of 20% to 35% for the daily dataset proposed by SeaWIFS and MODIS). Our method allows to reduce the temporal coverage issue since we compute the depleted area using values averaged over ∼2 months. Moreover it allows to cope with the intermediate convection issue since it is based on a linear relationship determined from all the convection cases obtained in the model over a 38-year period. In Section 3.1, we determined values of the coefficient by which we multiply the chlorophyll depleted area in the range of [751,1057] m for respectively V_{MLD} and $\tau_{29.11}$, i.e. not implying that convection obligatorily reaches the bottom under the chlorophyll depleted area. Computing the depleted area by using surface chlorophyll concentration values averaged over ∼2 months instead of instantaneous values enables to consider the full range of convection cases. Averaging the surface chlorophyll concentration indeed allows to integrate both spatial and temporal information about the intensity of the convection : deeper convection cases will be associated to longer durations, hence to chlorophyll depleted areas of larger extension, that will be observed during a longer period (and inversely).

The method proposed in this studies has however some weaknesses.

First, as seen above, comparison with atmospheric heat loss and previous observation and modeling studies suggests that DWF indicators time series obtained from satellite data underestimate or overestimate DWF in some cases.

Time series from satellite chlorophyll concentration seem to overestimate DWF for 2006 and 2013, and underestimate it for 2012 (Fig. 3). This is due to the particular chronology of those convection events. Fig. 10 shows the daily evolution of the mixed volume and average SLA and SST over the NWMS during winters for which HL_{DJF} is stronger than the average. 2006 and 2013 are not the most convective years in terms of volumes, however in 2006 the convection begins very early, and for both years it lasts throughout the winter with several peaks. The surface is therefore depleted in chlorophyll during a long time, and the resulting A_{lowCHL} is high for satellite observations. The model does not reproduce this. This is due to an overestimation of the modeled chlorophyll concentration during the periods and in the regions of low convection that results in an underestimation of A_{lowCHL}. Using in situ and satellite observations, *Auger et al.* [2014] indeed showed that the model tends to overestimate the winter chlorophyll concentration (February - mid March, their Figures 3 and 5). This chlorophyll concentration overestimation is seen on time series and maps of winter average chlorophyll modeled concentration : the mean chlorophyll concentration during the period January 25th - March 21st is overestimated by respectively 70% and 20% for 2006 and 2013, and generally for years of weak convection before 2005 (Fig. 5); the regions outside the depleted area show a positive chlorophyll concentration bias in the model (Fig. 1 and 6). In 2012, the second most convective event in the simulation in terms of volumes, the convection event is very short compared to other years, leading to an underestimation of A_{lowCHL} hence of DWF, both in model and in data.

Time series from altimetry SLA seems to underestimate 2006, 2010 and 2013 and overestimate 2012 (Fig. 3). This is not detected in the time series obtained from model SLA. This is related to the high frequency variability of SLA. Discrepancies between the modeled and satellite SLA are due partly to the representation of the steric effect in the model, which is computed from monthly fields (Sec. 2.1). High frequency variations of the steric effect that can for example be induced by a sudden surface cooling/warming are therefore not included in the model. In average, since we consider the average SLA over the period 15/02-15/03, the impact is limited, but for some particular cases it can impact the computation of A_{lowSLA}. Though 2012 is not the strongest convective year, the surface is very cold between 15/02 and 15/03 (see Fig. 10). This cooling seems to be captured by the altimetry data, that contains the real steric effect. In 2006, 2010 and 2013, on the contrary, there are several warm events between 15/02 and 15/03. As a result the altimetry SLA is not very low, resulting in an underestimation of A_{lowSLA} hence of the DWF indicators, which again is not captured by the model.

Second, the relationships between DWF, SLA and chlorophyll concentration were established from the model results. As seen above, this model shows some weaknesses in the representation of physical and biogeochemical processes and of their interactions. The established relationships are therefore not completely adapted for real altimetry and chlorophyll concentration data. Applying corrective methods detailed in Sec. 4.1 and 4.2 when applying the linear relationships found in the model to the real dataset partly corrected those weaknesses. However increasing the realism of the coupled model is essential to increase the ability of the linear relationships establish in the model to represent the real physical interactions between DWF, SLA and chlorophyll concentration. The performance of the coupled model should be improved in particular by recalibrating biogeochemical model parameters on the 2012-2013 well documented period, and by providing daily variable lateral boundary conditions to the physical model in order to better represent the steric effect high frequency.

Third, results from the numerical model have by definition a complete and high resolution spatial and temporal coverage. On the contrary, the coverage of satellite data is not perfect, due to the spatial and temporal resolution of the measurements and to external factors that hinders the measurements. Altimetry tracks are indeed spaced by several days and hundreds of kilometers in the NWMS, and ocean color data, though made daily at a high spatial resolution, are strongly impacted by cloud cover, showing an average coverage of 20% to 35%. These weaknesses of satellite data coverage can impact their ability to capture correctly the high frequency variations of SLA and chlorophyll concentration and participate to the misrepresentation of some DWF cases. The precision and accuracy of the satellite measurements and of the algorithms used to produce the data are an additional source of uncertainty in our time series.

Fourth, this study is based on the hypothesis that there is a strong linear relationship between DWF, SLA and chlorophyll concentration. The reality is of course more complex, and SLA and chlorophyll concentration are impacted by other factors. The source of uncertainty linked to the linear fitting was estimated by giving the value of the NRMSE and correlation between time series computed directly from the model results, and computed by applying the relationships to the model SLA and chlorophyll outputs : NRMSE varies between 10 and 15%, and correlation factors between 0.64 and 0.89 (SL>0.99). In particular, by construction, MLD_{mean} is a less integrated indicator than $\tau_{29.11}$ and V_{MLD}, which take into account both the depth and the area impacted by deep convection. The physical link between MLD_{mean} and the SLA and chlorophyll concentration is therefore less direct than for the volumic indicators. This explains that its correlation with A_{lowCHL} and A_{lowSLA} (resp. 0.64 and 0.75, Fig. 7), though still significant at more than 0.999, is weaker than for the other indicators. This, associated to difference between the model and observed SLA in terms of steric effect temporal averaging, explains the weak correlation obtained between the time series obtained from altimetry data and HL_{DJF} (Tab. 2 and Fig. 3). For the time series obtained from ocean color data on the contrary, MLD_{mean}

produces the highest correlation with HL_{DJF} (0.67 (SL>0.99), though the correlation between A_{lowCHL} and MLD_{mean} is the weakest of all (Fig. 7). The link between the atmospheric heat flux and the primary production is actually not only due to the effect of vertical mixing induced by cold atmospheric events on chlorophyll concentration, but also to the influence of the surface layer temperature, that largely depends on atmospheric heat flux, on primary production [*Herrmann et al.*, 2014]. This high correlation between chlorophyll concentration and atmospheric heat loss is therefore not associated here to the ability of ocean color data to capture MLD_{mean} interannual variability.

In this method we use altimetry and ocean color data as proxies of DWF. Since DWF results from surface buoyancy loss, that is mostly associated to cooling in the NWMS [*Herrmann et al.*, 2010], one could consider using sea surface temperature (SST) as a proxy of DWF, similarly as what we did for SLA and chlorophyll concentration. However the correlation between the winter SST and DWF indicators is much lower (<0.50) and less significant in our simulation than the correlations between winter SLA and chlorophyll concentration and DWF indicators. This is due to several reasons. First the temperature does not decrease regularly with depth in the NWMS, due to the presence of the warm Levantine Intermediate Water (LIW) between the colder surface Modified Atlantic Water (MAW) and Western Mediterranean Deep Water. When the mixed layer deepens, the temperature consequently first increases when reaching the LIW, then decreases. Second, atmospheric events, but also advection of cold and fresh (due to the Rhone river input) thus light water produced on the Gulf of Lions shelf toward the open sea can induce strong but brief cooling events of surface water in the convection area, not necessarily associated to DWF. Those results suggest that determining a SST criteria and building a DWF indicator from SST satellite data would not be possible.

6. Conclusion

Estimations of volume of dense water produced by deep convection and of its interannual and long term variability is of primary importance for the study of ocean circulation. Our objective in this paper was to propose a method allowing to assess the interannual variability of DWF using multi-sensors gridded data altimetry and ocean color data, taking the case of the NWMS which can be considered as a golden case study of DWF. For that, we used the results of a 38-year hydrodynamical simulation and biogeochemical simulations performed over the NWMS with the hydrodynamical-biogeochemical coupled high resolution model SYMPHONIE-Eco3m-S. We were able to establish linear relationships between DWF and sea surface height and chlorophyll concentration, based on the statistically significant correlations computed in the model between the areas of low SLA and low surface chlorophyll concentration in winter on one side, and the DWF intensity estimated in terms of depth and volumes of affected water (mean MLD, mixed volume and volume of newly formed dense water) on the other side. Relationships established here between DWF and SLA/surface chlorophyll concentration are not empirical but are obtained from a model that reproduces realistically the physical links between the ocean dynamics and the biogeochemistry. Using a 4 times longer simulation at a twice higher resolution than *Herrmann et al.* [2009], including in particular the period 2005-2013 with several convective years (see Fig. 3), we increased the robustness of those relationships. We then applied those relationships to time series of areas of low SLA and low surface chlorophyll concentration computed respectively from SSALTO-DUACS altimetry 24-year dataset and SeaWIFS and MODIS ocean color data. SeaWIFS and MODIS time series were merged to produce a 19-year time series. The chlorophyll concentration bias between the model results and the data was taken into account by adapting the threshold used to compute the depleted area to the observed dataset. The smoothing effect of the gridded altimetry data was taken into account by applying a multiplying corrective factor. This allowed us to produce for NWMS DWF indicators in terms of depth and volumes the first long time series covering the last 2 decades from observations. By comparison with existing estimations of DWF indicators and with the interannual variability of atmospheric heat loss over the region, we showed that the time series obtained from SSALTO-DUACS and the combined standard ocean color time series reproduce well the interannual variability of DWF. Comparison with estimations from in-situ observations suggests that those time series reproduce correctly the range of DWF indicators. We discussed the interest but also the weaknesses and uncertainties of our method (misrepresentation of several DWF cases, realism of the linear relationships; ability of the numerical model to represent realistically the physical and biogeochemical processes, their interactions and their variability; spatio-temporal coverage, accuracy and precision of the satellite data).

Using a combination of altimetry and ocean color data by applying bi-linear relationships does not significantly the interannual variability of the resulting DWF indicators time series. This is due to the fact that correlations between the predicted and direct time seris for a given DWF indicator are significantly different for A_{lowSLA} and A_{lowCHL}. Using bi-linear relationships could however be more efficient if those correlations were higher and more similar, which could be obtained when correcting some model biases in the representation of those variables.

Smoothing effect of gridded altimetry data should disappear in the SWOT wide-swath satellite altimetry mission (Surface Water and Ocean Topography, from 2020), that will provide sea level data with a complete spatial coverage at a much higher resolution. This should allow to increase significantly the quality of the DWF indicators time series obtained from altimetry dataset.

Our method is not proposed as a replacement of in-situ measurement. Indeed in-situ measurements methods dedicated to the observation of water masses in DWF sites are necessary to estimate the volume of those water masses and to evaluate and correct the models used to study and forecast DWF, hence to build our method. However satellite data are highly complementary to in-situ measurements given the length and quality of their spatial and temporal coverage, that would be too expensive to be reached through in-situ measurements, and that allow to monitor the interannual and long term evolution of processes implied in ocean circulation like DWF.

The feasibility of this method was examined for the NWMS convection region, but deep convection occurs in other regions of the world ocean, in particular the Greenland and Labrador seas. Deep water masses formed in those regions play an key role in the Atlantic and global ocean circulation. Numerical simulations suggested a weakening of global overturning circulation due to a decrease of dense water formation under the influence of climate change. Long term quantitative monitoring of DWF in deep convection regions of the world ocean, and the potential detection of a long term trend is therefore of great importance. Our method, applied to those regions, could contribute to this monitoring.

Acknowledgments. This work is a contribution to the MISTRALS/HyMeX and MISTRALS/Mermex programmes. It has received funding from the French National Research Agency (ANR) projects ASICS-MED (contract ANR-12-BS06-0003) and Additional support during the writing phase was provided by the Instituto Milenio de Oceanografa (IMO-Chile), funded by the Iniciativa Cientfica Milenio (ICM-Chile). We warmly thank the researchers that provided their estimations of DWF rates, with the discussions that we had together. Standard L3 near-surface chlorophyll-a concentrations daily SeaWIFS and MODIS are available on http://oceandata.sci.gsfc.nasa.gov. SSALTO/DUACS DT and NRT data are distributed by the Copernicus Marine and Environment Monitoring Service (CMEMS, http://marine.copernicu.eu). Results from numerical simulations are available on request (marine.herrmann@ird.fr).

References

Auger, P.-A., F. Diaz, C. Ulses, C. Estournel, J. Neveux, F. Joux, M. Pujo-Pay, and J. Naudin (2011), Functioning of the planktonic ecosystem of the Rhone river plume (NW Mediterranean) during spring and its impact on the carbon export: a field data and 3-D modelling combined approach., *Biogeosciences*, *8*, 3231–3261, doi:10.5194/bg-8-3231-2011.

Auger, P.-A., C. Estournel, C. Ulses, L. Stemmann, S. Somot, and F. Diaz (2014), Interannual control of plankton ecosystem in a deep convection area as inferred from a 30-year 3D modeling study : winter mixing and prey/predator interactions in the NW

Mediterranean, *Progress in Oceanography*, pp. 12–27, doi:10.1016/j.pocean.2014.04.004.

Béthoux, J.-P., X. Durrieu de Madron, F. Nyffeler, and D. Tailliez (2002), Deep water in the western Mediterranean : peculiar 1999 and 2000 characteristics, shelf formation hypothesis, variability since 1970 and geochemical inferences, *J. Mar. Syst.*, *33-34*, 117–131.

Bosc, E., A. Bricaud, and D. Antoine (2004), Seasonal and interannual variability in algal biomass and primary production in the Mediterranean Sea, as derived from 4 years of SeaWifs observations, *Global Biogeochemical Cycles*, *18* (GB1005).

Bosse, A. (2015), Circulation générale et couplage physique-biogéochimie á (sous-) mésoechélle en Méditerranée Nord-Occidentale á partir de données in situ, Ph.D. thesis, Université Paris 6 - Pierre et Marie Curie.

Bouffard, J., S. Vignudelli, M. Herrmann, F. Lyard, P. Marsaleix, Y. Ménard, and P. Cipollini (2008), Comparison of ocean dynamics with a regional circulation model and improved altimetry in the northwestern mediterranean, *Terr., Atm. and Oc. Sciences*, *19*, doi:10.3319/TAO.2008.19.1-2.117(SA).

Conan, P. (2013), DEWEX-MERMEX 2013 LEG2 cruise, RV Le Suroit, doi: 10.17600/13020030.

de Lavergne, C., J. Palter, E. Galbraith, R. Bernardello, and I. Marinov (2014), Cessation of deep convection in the open Southern Ocean under anthropogenic climate change, *Nature Climate Change*, *4*, 278282, doi:10.1038/nclimate2132.

D'Ortenzio, F., and M. Ribera d'Alcalà (2009), On the trophic regimes of the Mediterranean Sea: a satellite analysis., *Biogeosciences*, *6*, 139–148.

Durrieu de Madron, X., L. Houpert, P. Puig, A. Sanchez-Vidal, P. Testor, A. Bosse, C. Estournel, S. Somot, F. Bourrin, M. N. Bouin, M. Beauverger, L. Beguery, A. Calafat, M. Canals, C. Cassou, L. Coppola, D. Dausse, F. DOrtenzio, J. Font, S. Heussner, S. Kunesch, D. Lefevre, H. L. Goff, J. Martn, L. Mortier, A. Palanques, and P. Raimbault (2013), Interaction of dense shelf water cascading and open-sea convection in the northwestern Mediterranean during winter 2012, *Geophys. Res. Lett.*, *40*, 13791385, doi:10.1002/grl.50331.

Estournel, C., P. Testor, P. Damien, F. DOrtenzio, P. Marsaleix, P. Conan, F. Kessouri, X. Durrieu de Madron, L. Coppola, J.-M. Lellouche, S. Belamari, L. Mortier, C. Ulses, M.-N. Bouin, and L. Prieur (2016), High resolution modelling of dense water formation in the north-western Mediterranean: benefits from an improved initial state in summer, *J. Geophys. Res.*, doi:10.1002/2016JC011935.

Gelderloos, R., C. A. Katsman, and K. Vage (2013), Detecting labrador sea water formation from space, *Journal of Geophysical Research: Oceans*, *118*(4), 2074–2086, doi:10.1002/jgrc.20176.

Greatbatch, R. J. (1994), A note on the representation of steric sea level in models that conserve volume rather than mass., *J. Geophys. Res.*, *99*, 12,767–12,771.

Herrmann, M., and S. Somot (2008), Relevance of ERA40 dynamical downscaling for modeling deep convection in the Mediterranean Sea, *Geophys. Res. Lett.*, *35(L04607)*, doi:10.1029/2007GL032442.

Herrmann, M., S. Somot, F. Sevault, C. Estournel, and M. Déqué (2008), Modeling the deep convection in the Northwestern Mediterranean sea using an eddy-permitting and an eddy-resolving model: case study of winter 1986-87, *J. Geophys. Res.*, doi:

10.1029/2006JC003991.

Herrmann, M., J. Bouffard, and K. Béranger (2009), Monitoring open-ocean deep convection from space, *Geophys. Res. Lett.*, *36(L03606)*, doi:10.1029/2008GL036422.

Herrmann, M., F. Sevault, J. Beuvier, and S. Somot (2010), What induced the exceptional 2005 convection event in the northwestern Mediterranean basin ? Answers from a modeling study, *J. Geophys. Res.*, *115(C08029)*, doi:10.1029/2009JC005749.

Herrmann, M., F. Diaz, C. Estournel, P. Marsaleix, and C. Ulses (2013), Impact of atmospheric and oceanic interannual variability on the Northwestern Mediterranean Sea pelagic planktonic ecosystem and associated carbon cycle., *J. Geophys. Res.*, *118*, 1–22, doi:10.1002/jgrc.20405.

Herrmann, M., C. Estournel, F. Diaz, and F. Adloff (2014), Impact of climate change on the Northwestern Mediterranean Sea pelagic planktonic ecosystem and associated carbon cycle., *J. Geophys. Res.*, *119*, 5815–5836, doi:10.1002/2014JC010016.

Houpert, L., X. Durrieu de Madron, P. Testor, A. Bosse, F. DOrtenzio, M.-N. Bouin, D. Dausse, H. Le Goff, S. Kunesch, M. Labaste, L. Coppola, L. Mortier, and P. Raimbault (2016), Observations of Open-Ocean Deep Convection in the Northwestern Mediterranean Sea : Seasonal and Interannual Variability of Mixing and Deep Water Masses for the 2007-2013 Period., *Journal of Geophysical Research*, doi: 10.1002/2016JC011857.

Kalnay, E., M. Kanamitsu, R. Kistler, W. Collins, D. Deaven, L. Gandin, M. Iredell, S. Saha, G. White, J. Woollen, Y. Zhu, A. Leetmaa, B. Reynolds, M. Chelliah, W. Ebisuzaki, W. Higgins, J. Janowiak, K. Mo, C. Ropelewski, J. Wang, R. Jenne, and D. Joseph (1996), The NCEP/NCAR 40-year reanalysis project, *Bull. Amer. Me-*

teor. Soc., *77*, 437–471.

Léger, F., C. Lebeaupin Brossier, H. Giordani, T. Arsouze, J. Beuvier, M.-N. Bouin, E. Bresson, V. Ducrocq, N. Fourrié, and M. Nuret (2016), Dense Water Formation in the North-Western Mediterranean area during HyMeX-SOP2 in 1/36 ocean simulations: Sensitivity to initial conditions, *Journal of Geophysical Research*, doi: 10.1002/2015JC011542.

Lombard, A., A. Cazenave, P. Y. L. Traon, and M. Ishii (2005), Contribution of thermal expansion to present-day sea-level change revisited, *Global Planetary Change*, *47*, 1–16.

Marsaleix, P., F. Auclair, J. W. Floor, M. J. Herrmann, C. Estournel, I. Pairaud, and C. Ulses (2008), Energy conservation issues in sigma-coordinate free-surface ocean models, *Ocean Modelling*, *20*, 61–89, doi:10.1016/j.ocemod.2007.07.005.

Marsaleix, P., C. Ulses, I. Pairaud, M. J. Herrmann, J. W. Floor, C. Estournel, and F. Auclair (2009), Open boundary conditions for internal gravity wave modelling using polarization relations, *Ocean Modelling*, *29*, 27–42, doi:10.1016/j.ocemod.2009.02.010.

Marshall, J., and F. Schott (1999), Open-ocean convection: observations, theory, and models, *Rev. Geophys.*, *37*(1), 1–64.

O'Reilly, J., and et al. (2000), SeaWiFS Postlaunch Calibration and Validation Analyses, Part 3., *Tech. Rep. 2000-206892,11*, NASA Goddard Space Flight Center, 49pp.

Schroeder, K., A. Ribotti, M. Borghini, R. Sorgente, A. Perilli, and G. P. Gasparini (2008), An extensive western Mediterranean deep water renewal between 2004 and 2006, *Geophys. Res. Lett.*, *35, L18605*, doi:10.1029/2008GL035146.

Somot, S., F. Sevault, and M. Déqué (2006), Transient climate change scenario simulation of the Mediterranean Sea for the 21st century using a high resolution ocean circulation model, *Clim. Dyn.*, pp. 1 – 29, doi:10.1007/s00382-006-0167-z.

Somot, S., L. Houpert, F. Sevault, P. Testor, A. Bosse, I. Taupier-Letage, M. Bouin, R. Waldman, C. Cassou, E. Sanchez-Gomez, X. Durrieu de Madron, F. Adloff, P. Nabat, and M. Herrmann (2016), Characterizing, modelling and understanding the climate variability of the deep water formation in the North-Western Mediterranean Sea, *Climate Dynamics*, doi:10.1007/s00382-016-3295-0.

Testor, P. (2013), DEWEX-MERMEX 2013 LEG1 cruise, RV Le Suroit, doi: 10.17600/13020010.

Ulses, C., P.-A. Auger, K. Soetaert, P. Marsaleix, F. Diaz, L. Coppola, M.Herrmann, F. Kessouri, , and C. Estournel (2016), Budget of organic carbon in the North-Western Mediterranean Open Sea over the period 2004-2008 using 3D coupled physical-biogeochemical modeling, *Journal of Geophysical Research*, doi:10.1002/2016JC011818.

Waldman, R., S. Somot, M. Herrmann, P. Testor, C. Estournel, F. Sevault, L. Prieur, L. Mortier, L. Coppola, V. Taillandier, P. Conan, and D. Dausse (2016), Estimating dense water formation rates with an Observing System Simulation Experiment (OSSE): case study in the Northwestern Mediterranean sea., *Journal of Geophysical Research*, doi:10.1002/2016JC011694.

Yashayaev, I. (2007), Hydrographic changes in the Labrador Sea, 1960-2005, *Prog. Oceanogr.*, *73*, 242276, doi:10.1016/j.pocean.2007.04.015.

Table 1. Annual time series of DWF indicators between 1993 and 2016: MLD_{mean} (m), V_{MLD} (Sv) and $\tau_{29.11}$ (Sv) indicators predicted by applying the relationships established in Sec. 3.1, 3.2 and 3.3 to A_{lowCHL} and A_{lowSLA} computed from merged satellite ocean color data from SeaWIFS and MODIS and from the SSALTO/DUACS DT altimetry satellite data. When applying the equations to real satellite data, adjustment methods explained in Sec. 4.1 and 4.2 were used.

	altimetry			ocean color			Combined altimetry + ocean color		
year	MLD_{mean}	V_{MLD}	$\tau_{29.11}$	MLD_{mean}	V_{MLD}	$\tau_{29.11}$	MLD_{mean}	V_{MLD}	$\tau_{29.11}$
1993	980	0,00	0,00						
1994	1126	0,00	0,00						
1995	1116	0,00	0,00						
1996	1145	0,00	0,00						
1997	1198	0,00	0,00						
1998	157	0,00	0,00	1040	0,52	0,55	1037	0,47	0,53
1999	1160	0,00	0,00	1351	0,46	0,46	1183	0,41	0,44
2000	822	0,00	0,00	1104	0,35	0,31	847	0,32	0,30
2001	715	0,00	0,00	891	0,15	0,02	716	0,15	0,02
2002	929	0,00	0,00	883	0,19	0,08	898	0,18	0,08
2003	1346	0,96	1,14	945	0,19	0,09	1267	0,33	0,13
2004	738	0,00	0,00	1227	0,78	0,91	798	0,69	0,88
2005	1289	1,15	1,39	1908	2,05	2,69	1397	1,96	2,67
2006	1207	0,00	0,00	1481	1,79	2,33	1248	1,56	2,26
2007	839	0,00	0,00	874	0,00	0,00	819	0,00	0,00
2008	1395	0,00	0,00	880	0,16	0,03	1297	0,15	0,03
2009	1311	0,31	0,25	1119	0,39	0,36	1269	0,38	0,36
2010	679	0,00	0,00	1264	0,97	1,18	754	0,86	1,15
2011	1254	0,45	0,44	934	0,24	0,15	1186	0,28	0,17
2012	1402	2,90	3,76	1179	0,34	0,30	1359	0,80	0,44
2013	1234	0,00	0,00	1450	1,45	1,86	1264	1,27	1,80
2014	1290	0,45	0,45	873	0,00	0,00	1205	0,19	0,03
2015	1377	0,64	0,69	1028	0,50	0,52	1309	0,53	0,53
2016	1173	0,00	0,00	909	0,19	0,08	1111	0,18	0,08

Table 2. Correlation factors (with significant levels SL) between time series of HL_{DJF} computed from NCEP reanalysis [*Kalnay et al.*, 1996] and time series of DWF indicators given directly by the model, predicted by model chlorophyll concentration and ocean color data applying the linear equations established in Sec. 3.1, predicted by model SLA and altimetry data applying the linear equations established in Sec. 3.2, and predicted by combined model SLA and chlorophyll concentration and combined altimetry and ocean color data applying the bi-linear equations established in Sec. 3.3. When applying the equations to real satellite data, adjustment methods explained in Sec. 4.1 and 4.2 were used.

Predicted from	MLD_{mean}	V_{MLD}	$\tau_{29.11}$	period	length(years)
Direct model results	0.681 (> 0.999)	0.746 (>0.999)	0.707 (>0.999)	1976-2013	38
Modelled [chlorophyll]	0.777 (> 0.999)	0.669 (>0.999)	0.644 (>0.999)	1976-2013	38
average standard	0.667 (0.998)	0.583 (0.991)	0.568(0.989)	1998-2016	19
Modelled SLA	0.683 (>0.999)	0.685 (>0.999)	0.667 (>0.999)	1976-2013	38
SLA from altimetry	0.241 (0.744)	0.602 (0.998)	0.596 (0.998)	1993-2016	24
Modelled SLA+CHL	0.725 (>0.999)	0.682(>0.999)	0.647 (>0.999)	1976-2013	38
satellite SLA and CHL	0.434 (0.937)	0.687(>0.999)	0.594(0.993)	1998-2016	19

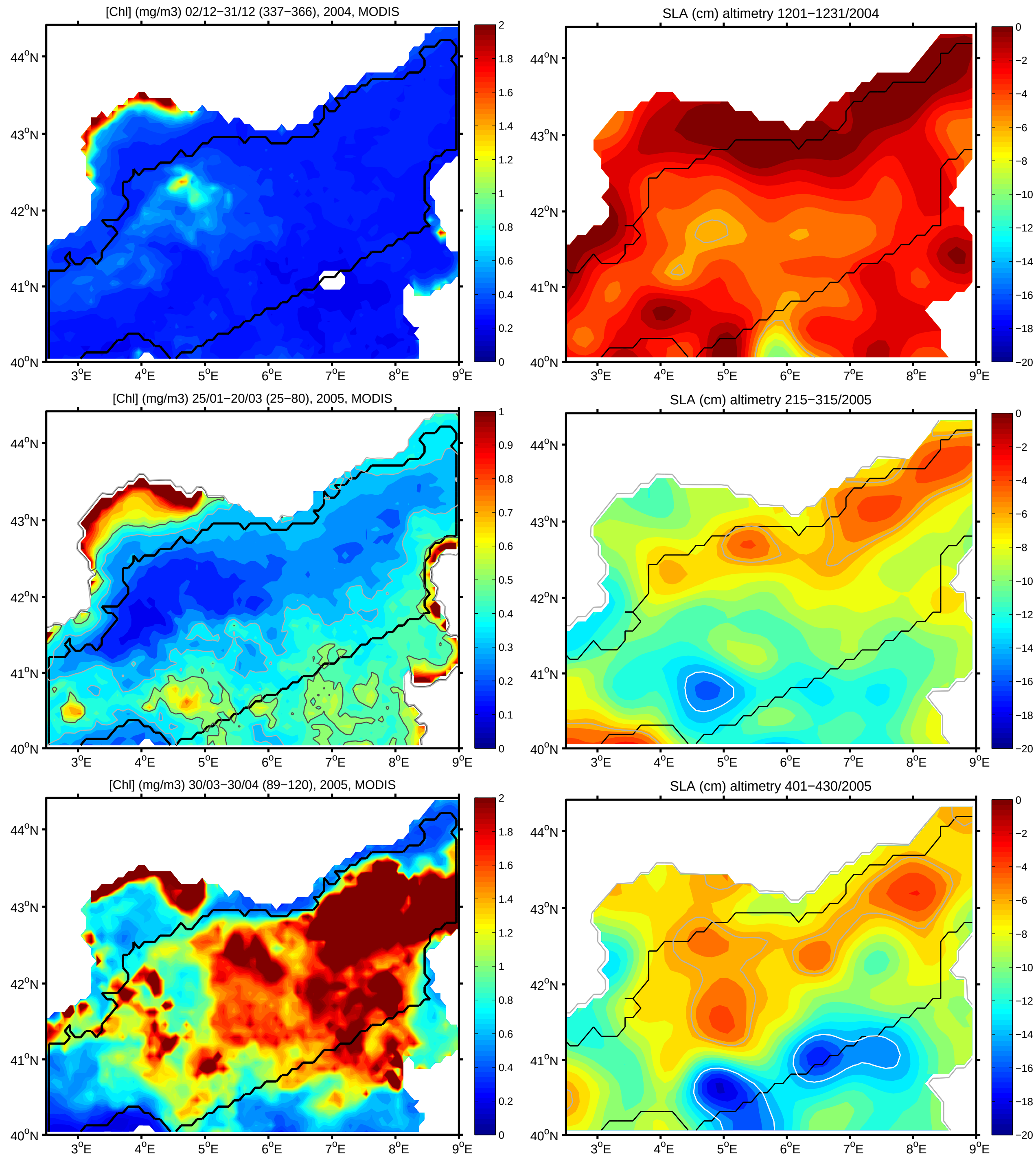

Figure 1. Sea surface chlorophyll concentration (mgChl.m^{-3}, left) and sea level anomaly (cm, right) for winter 2005 in satellite ocean color data and altimetry. From top to bottom : averages for December 2004 (top), between January 25th and March 21st, 2005 for chlorophyll concentration and February 15th and March 15th for SLA (middle), and for April 2005 (bottom). White line corresponds to the 0.35 mgChl.m^{-3} isoline for surface chlorophyll concentration. White, resp. gray, line corresponds to the -14 cm, resp. -5.5 cm, isoline for SLA. Black line corresponds to the limits of the region RDC where A_{lowChl} (defined in Eq. 5) and A_{lowSLA} (defined in Eq. 6) are computed.

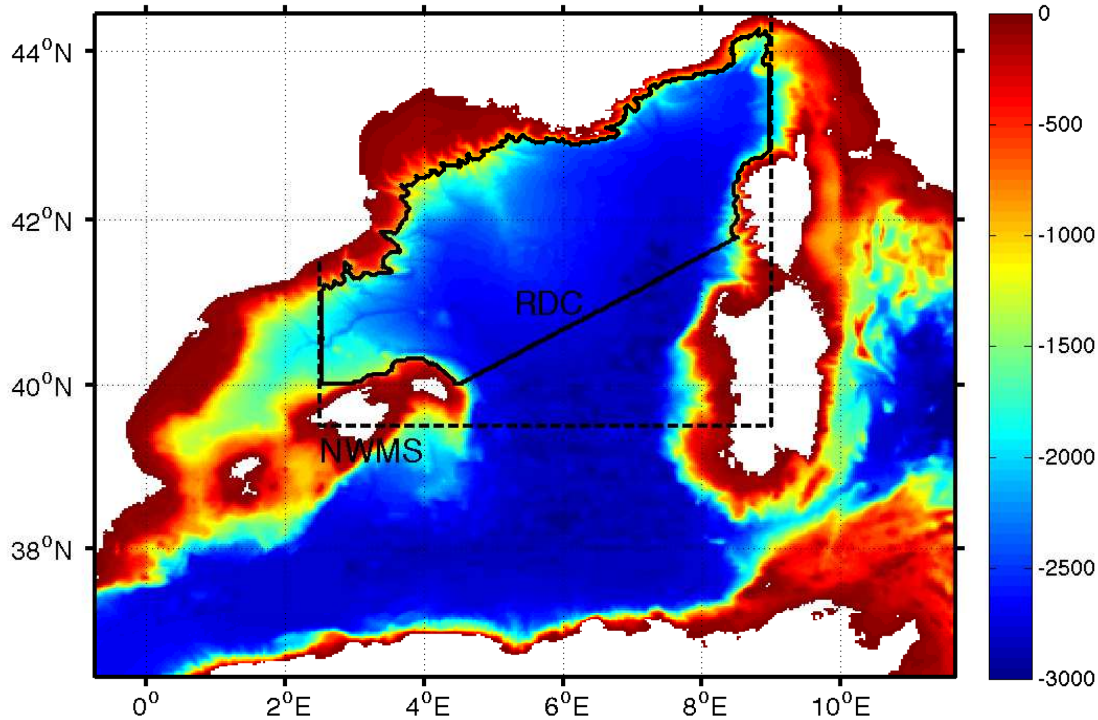

Figure 2. Bathymetry of the modelled domain (m). Black dotted line corresponds to the limits of the NWMS region, and black full line corresponds to the limits of the RDC region.

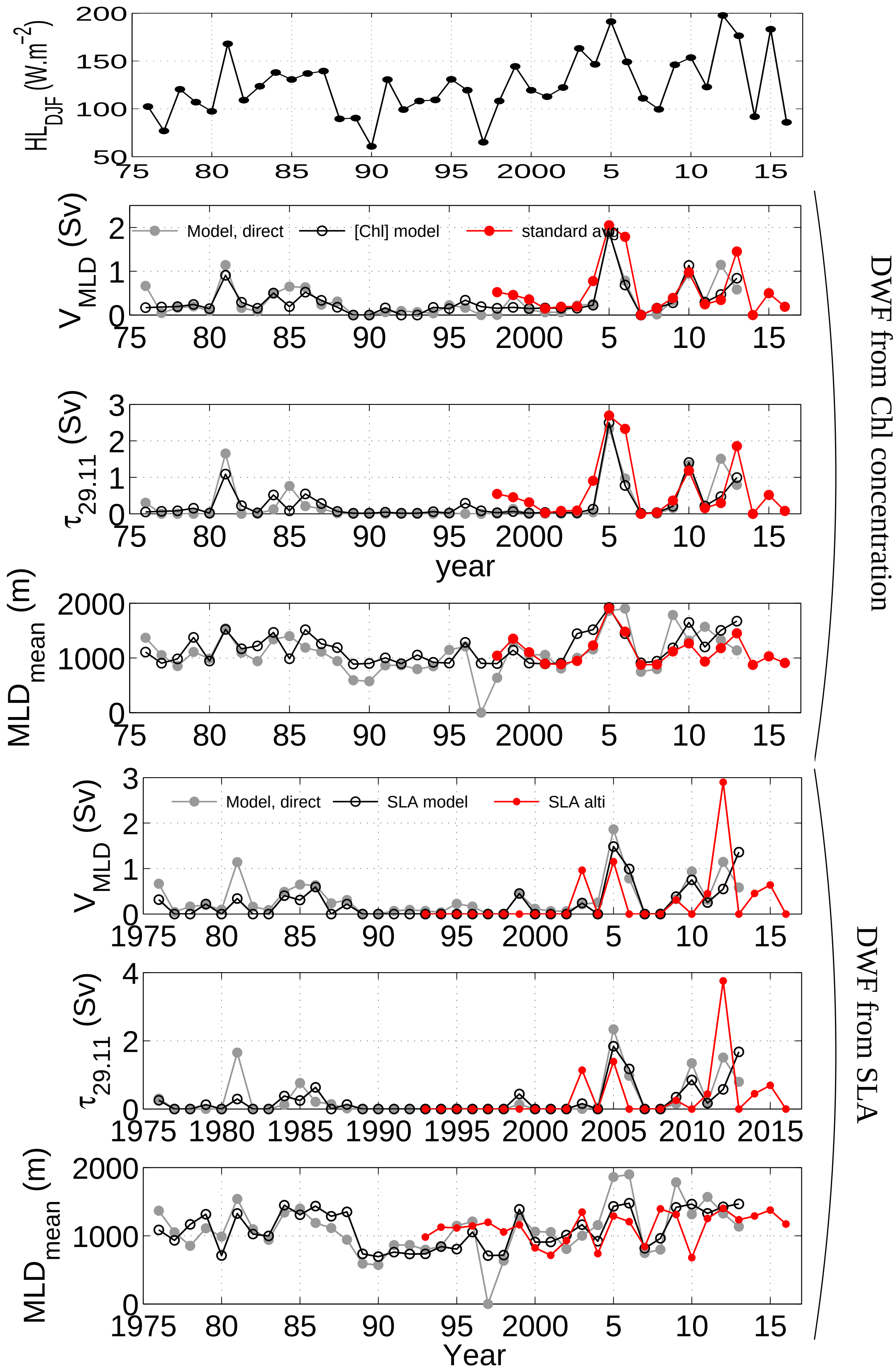

Figure 3. Annual time series of atmospheric and DWF indicators between 1975 and 2016. (top) Winter heat loss over the NWMS, HL_{DJF}, computed from NCEP reanalysis [*Kalnay et al.*, 1996]. (middle) DWF indicators V_{MLD}, $\tau_{29.11}$ and MLD_{mean} computed directly in the model (gray), and predicted by applying the relationships established in Sec. 3.2 to A_{lowCHL} computed in the model (black) and from merged satellite data from SeaWIFS and MODIS (red). (bottom) DWF indicators computed directly in the model (gray) and predicted by applying the relationships established in Sec. 3.1 to A_{lowSLA} computed in the model (black) and from the SSALTO/DUACS DT satellite data (red). When applying the equations to real satellite data, adjustment methods explained in Sec. 4.1 and 4.2 were used.

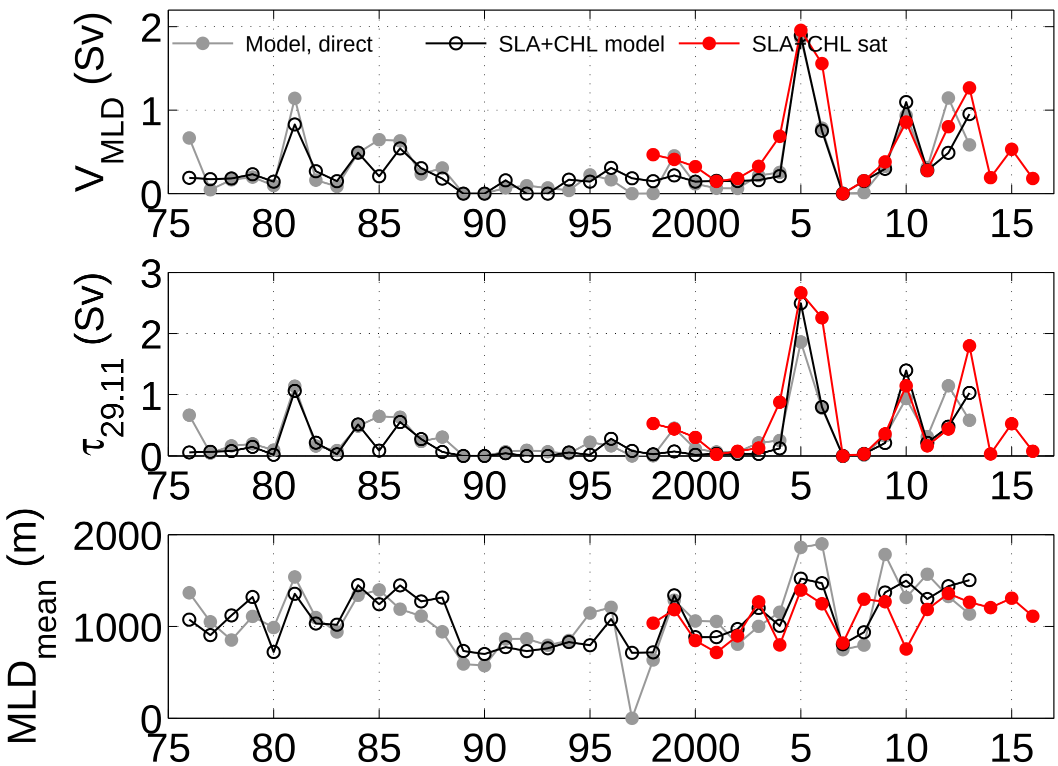

Figure 4. Annual time series of DWF indicators between 1975 and 2016: V_{MLD}, $\tau_{29.11}$ and MLD_{mean} indicators computed directly in the model (gray), and predicted by applying the multivariate relationships established in Sec. 3.3 to A_{lowCHL} and A_{lowSLA} computed in the model (black) and from merged satellite data from SeaWIFS and MODIS and from the SSALTO/DUACS DT satellite data (red). When applying the equations to real satellite data, adjustment methods explained in Sec. 4.1 and 4.2 were used.

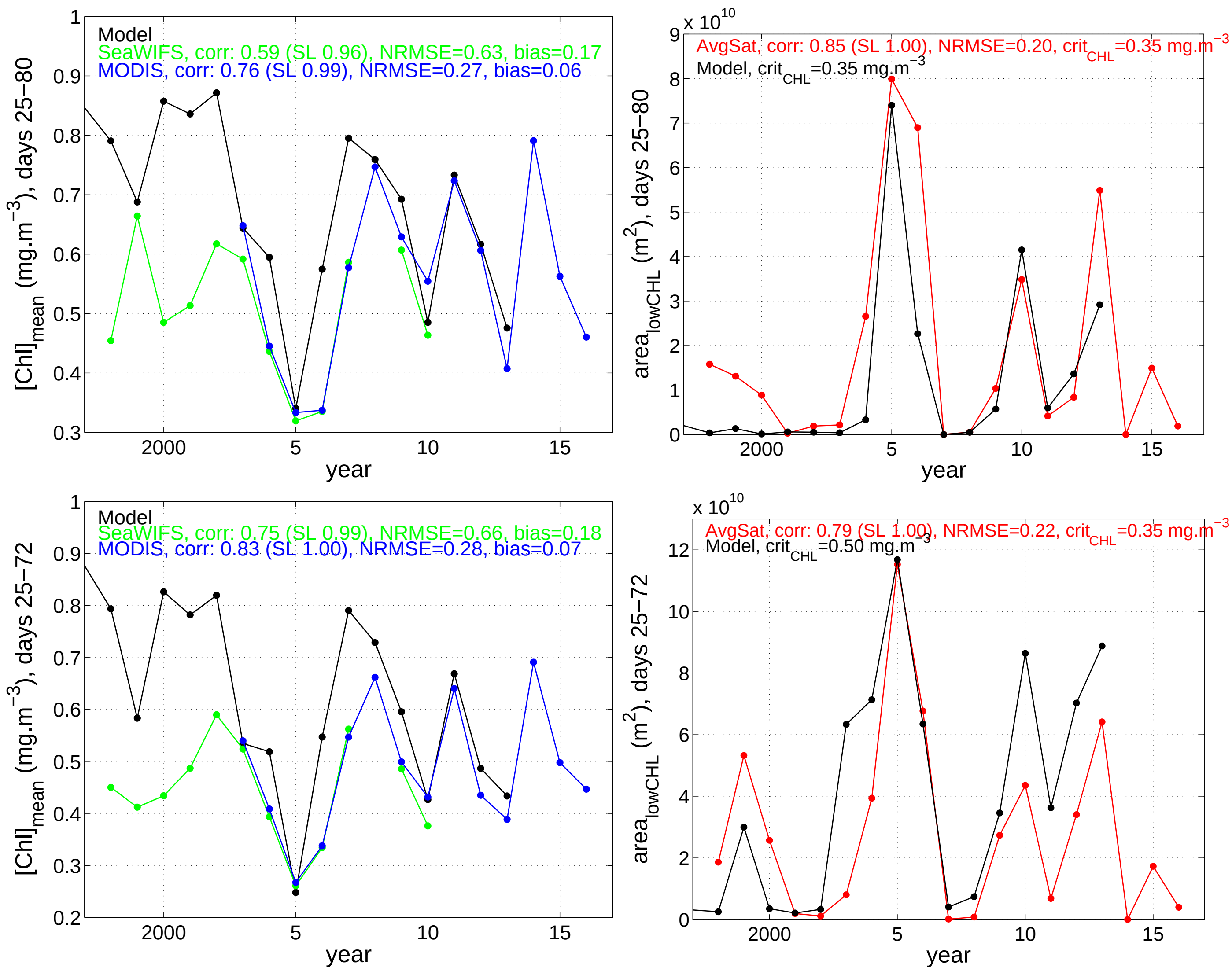

Figure 5. Comparison of surface chlorophyll concentration in the model and in the data. Annual time series of the surface chlorophyll concentration (mgChl.m^{-3}, left) and chlorophyll depleted area A_{lowCHL} (m^2, right) averaged over the region RDC and the period 25/01-21/03 (top) and the period 25/01-14/03 (bottom) computed in the model (black) and in the satellite data issued from SeaWIFS (green) and MODIS (blue). When computing A_{lowChl} from real satellite data, criteria adjustment explained in Sec. 4.1 is used.

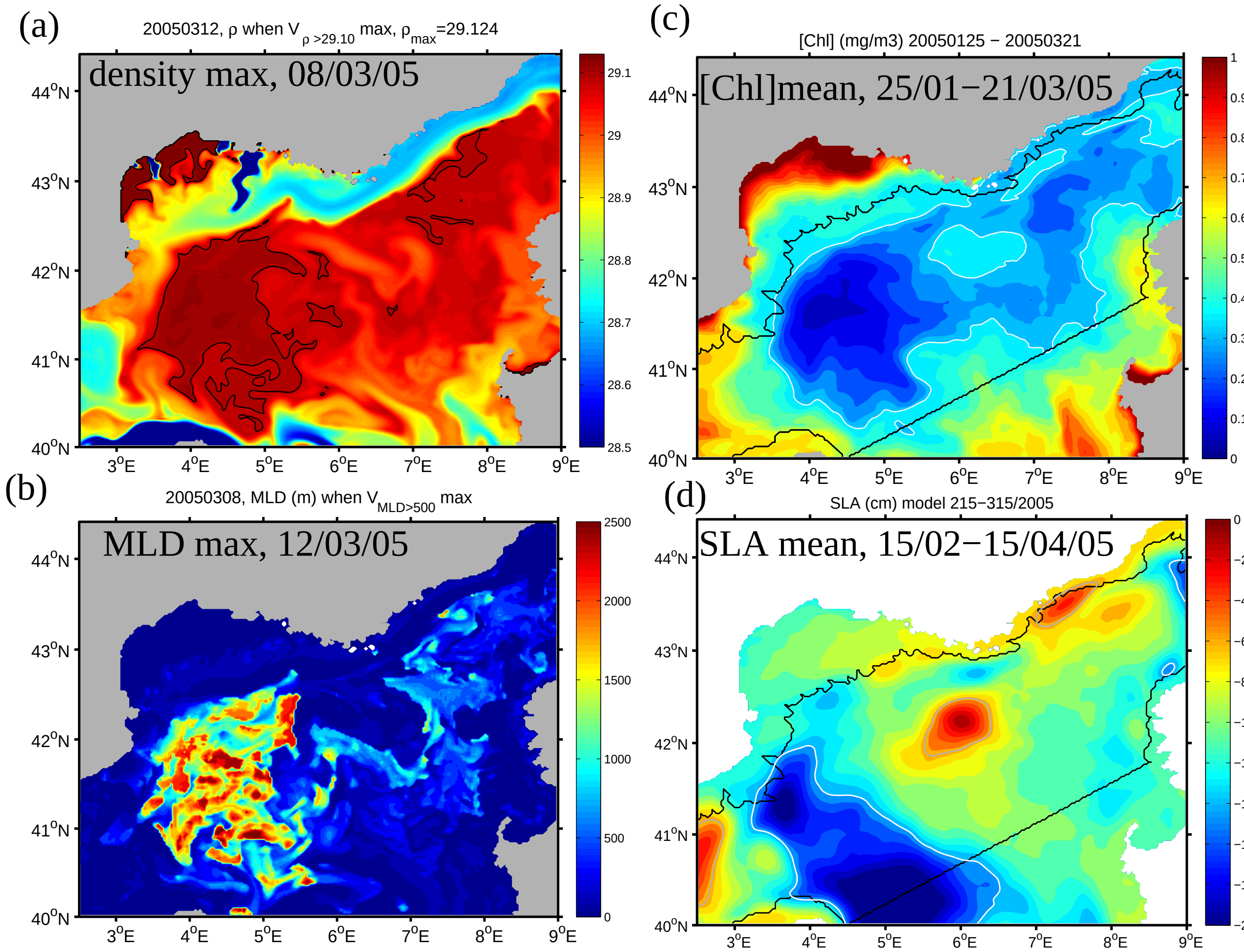

Figure 6. Sea surface characteristics for winter 2005 in the model. (a) Surface density (kg.m^{-3}) on the day when $V_{29.11}$ (defined in Eq. 4) is maximum. Dark grey lines corresponds to the 29.11 kg.m^{-3} isoline. (b) MLD (m) on the day when V_{MLD} (defined in Eq. 2) is maximum. White line corresponds to the 500 m isoline. (c) Surface chlorophyll concentration (mgChl.m^{-3}) averaged between January 25th and March 21st. Light grey line corresponds to the 0.35 mgChl.m^{-3} isoline. (d) SLA (cm) averaged between February 15th and March 15th. White, resp. gray, line corresponds to the -14.0 cm, resp. -5.5 cm, isoline. Black line correspond to the limits of the region RDC where A_{lowChl} (defined in Eq. 5) is computed.

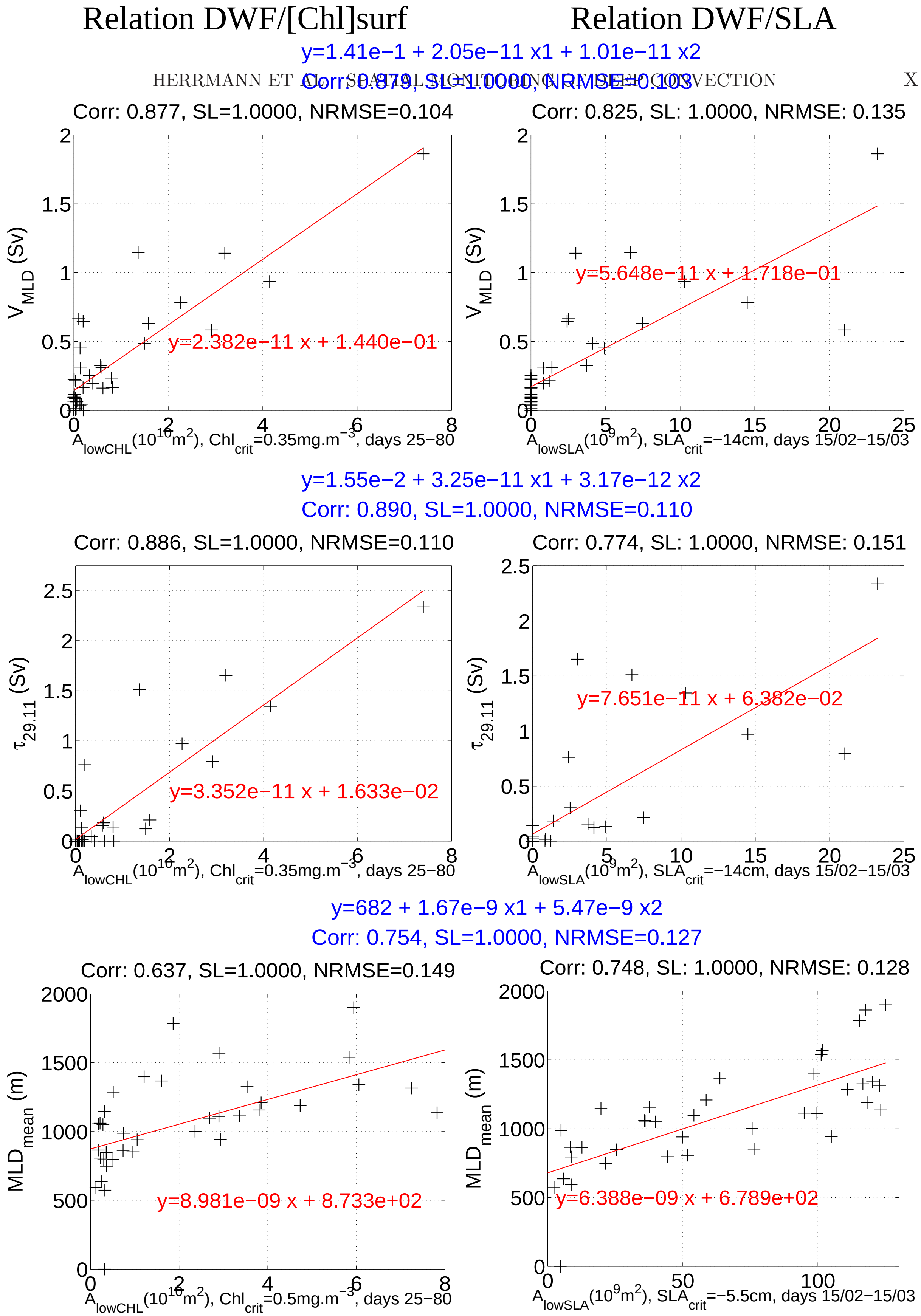

Figure 7. Relationships established in the model between the annual DWF intensity indicators V_{MLD} (top), $\tau_{29.11}$ (middle), MLD_{mean} (bottom), and the low surface chlorophyll concentration area A_{lowCHL} (left) and low SLA area A_{lowSLA} (right). For each indicator, bi-linear regression analysis coefficients and correlation and NRMSE of corresponding time series with direct modeled time series are indicated in blue.

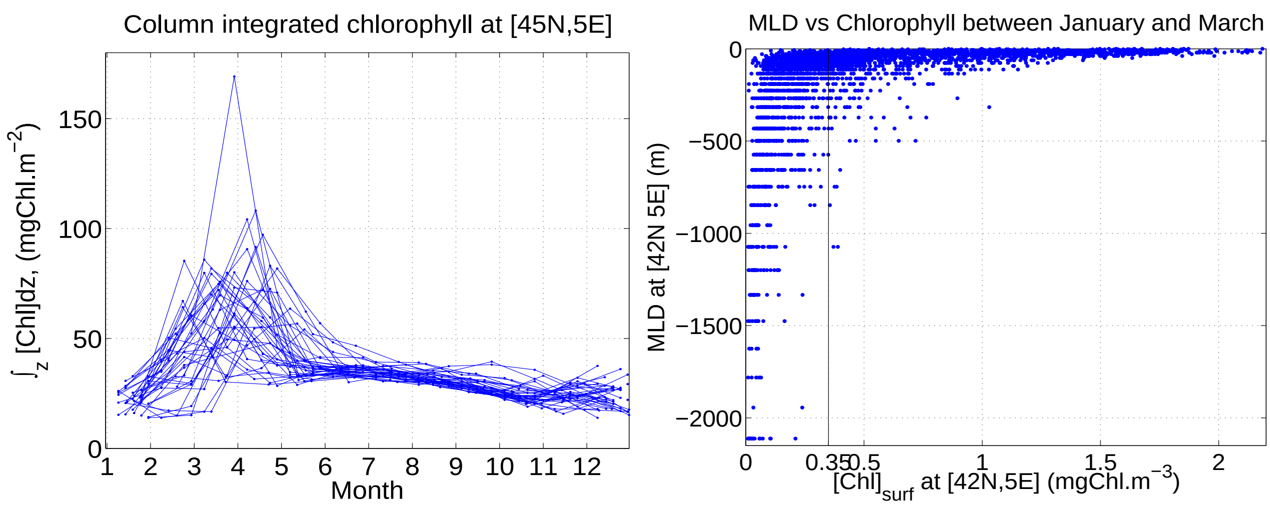

Figure 8. Relation between MLD and chlorophyll concentration in the model. (left) Annual evolution of the column-integrated chlorophyll content over the water column at [42°N 5°E] for the 38 years of the simulation. (right) Scatterplot of the daily values of MLD vs. surface chlorophyll concentration at the center of the convection area, [42°N 5°E], between January and March.

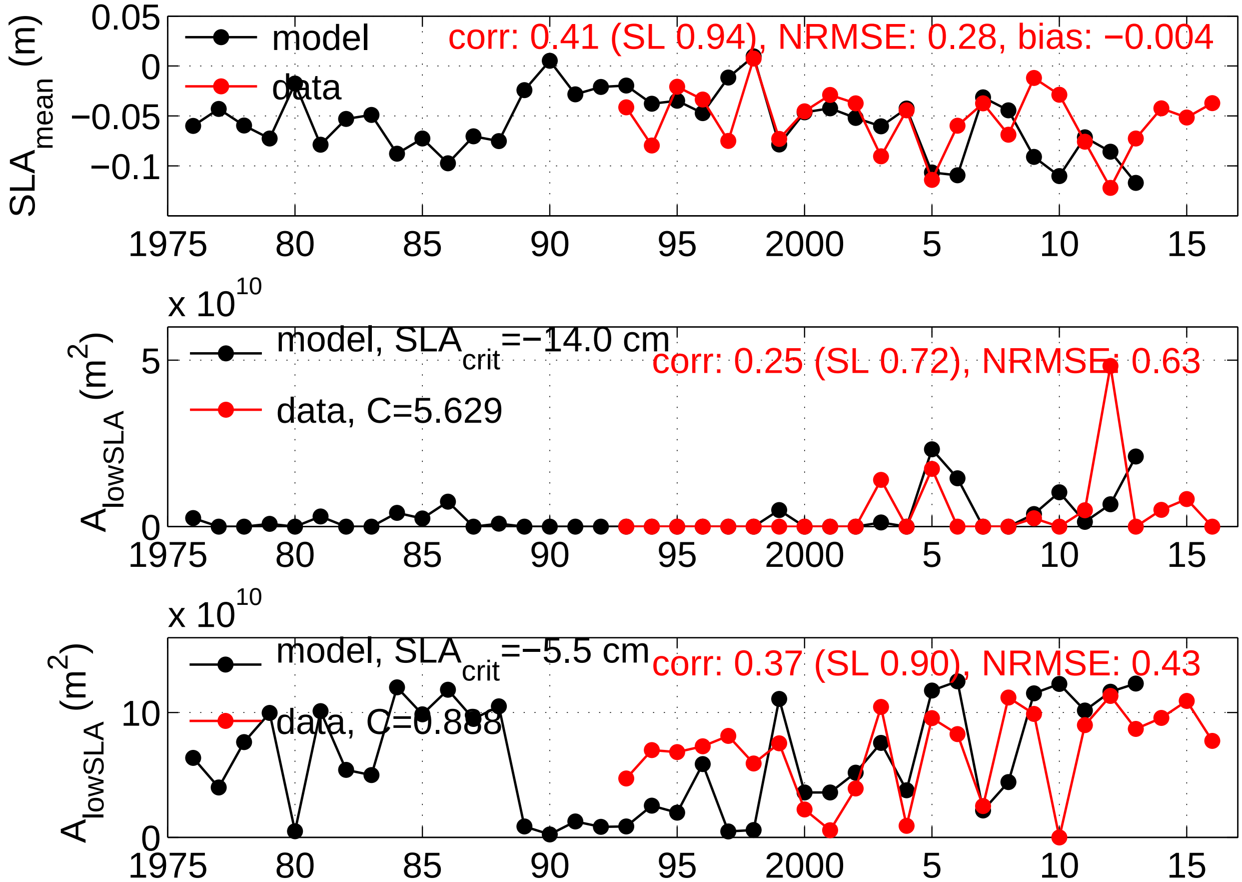

Figure 9. Comparison of SLA in the model and in the data. Annual time series of the average over February 15th-March 15th of the mean SLA over RDC (top) and of the low SLA area A_{lowSLA} computed in the model (black) and in the altimetry data (red) for $SLA_{crit} = -14.0$ cm (middle) and -5.5 cm (bottom). When computing A_{lowSLA} from altimetry, adjustment method explained in Sec. 4.2 is used.

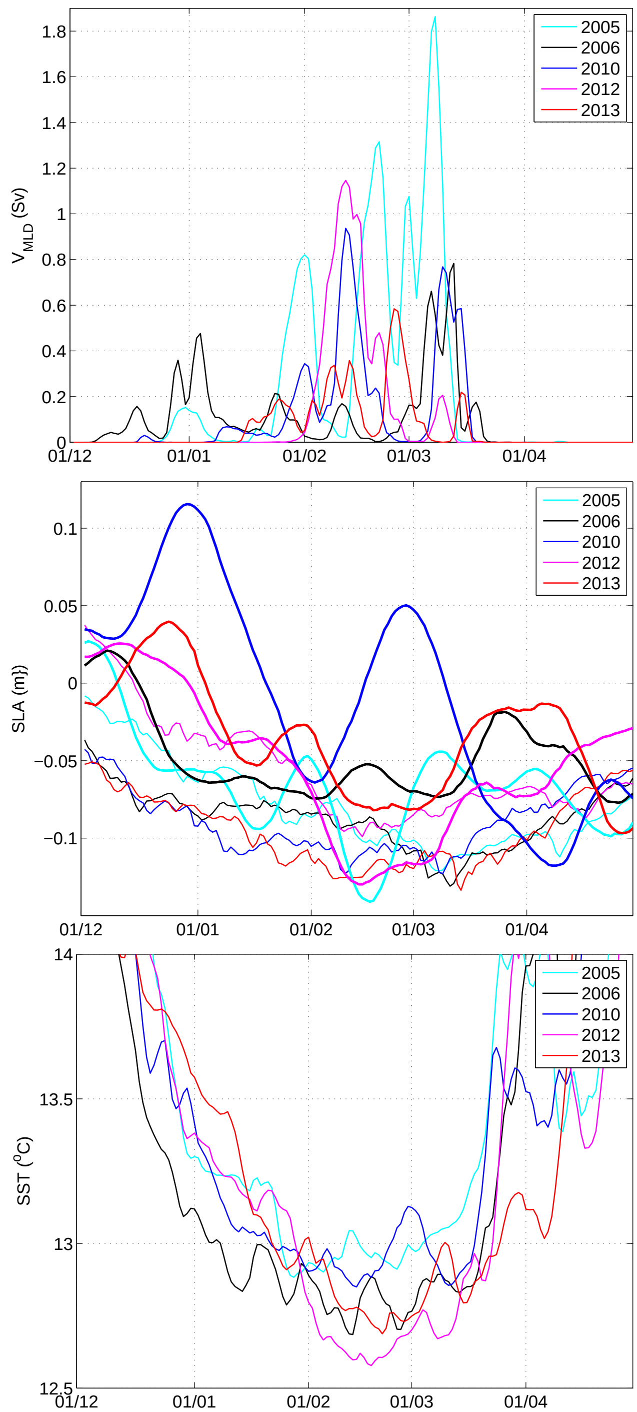

Figure 10. Evolution of the daily average mixed volume (top), SLA and SST averaged over the NWMS between December 1st and April 30th for winters 2004-05, 2005-06, 2009-10, 2011-12 and 2012-13.